Correlation between phosphorus segregation and stress corrosion cracking susceptibility in the heat affected zone of an A533B-A182 dissimilar weld joint

Graduate School of Engineering, Tohoku University	Ziqing ZHAI	Member
Graduate School of Engineering, Tohoku University	Hiroshi ABE	Member
Central Research Institute of Electric Power Industry	Yuichi MIYAHARA	Non-member
Graduate School of Engineering, Tohoku University	Yutaka WATANABE	Member

Effects of thermal history and segregation on the susceptibility of stress corrosion cracking (SCC) in the heat-affected zone (HAZ) of an alloy 182-A533B dissimilar weld joint in high temperature, oxygenated water doped with SO_4^{2-} and Cl^- was evaluated by creviced bent beam test. Results indicate that step cooling and the addition of Cl^- promoted SCC propagation and reactivation in HAZ. It is also suggested that compositional changes induced by welding and step cooling, especially the segregation of phosphorus at grain/packet boundaries and precipitate-matrix interfaces, played an important role in promoting SCC reactivation/propagation in HAZ.

Keywords: low alloy steel; phosphorus segregation; stress corrosion cracking; crack reactivation; BWR conditions.

1. Introduction

In boiling water reactors (BWR), the low alloy pressure vessel is the most critical pressure-boundary component as far as safety and plant life are concerned. In recent years, stress corrosion cracking (SCC) incidences in Ni-base alloy A182 portion of the dissimilar weld joints (DWJ) in core shroud supports has occurred in a number of BWR plants worldwide [1]. The tips of SCCs were usually located within the A182 weld metal but concerns have been raised on the possible growth of SCC across the fusion boundary (FB) into low alloy steel (LAS). From the extensive laboratory experiments followed up, fast propagation of interdendritic SCCs were found parallel to the solidification direction in the Ni-base weld metal. Most of the cracks ceased on the fusion boundary (FB) by pitting, but minor crack growth into the HAZ and reactivation of cracks from pitting were also occasionally observed [2-4]. Of particular interest is that the cracks in the heat-affected zone (HAZ) seem to favor grain boundaries (GBs) and are usually deflected when GBs intersect. This is indicative of the importance of microstructure in the intergranular (IG) SCC propagation and reactivation in HAZ.

Corresponding author: Ziqing Zhai
Address: 6-6-01-2 Aoba, Aramaki, Aoba-Ku, Sendai 980-8579, Miyagi
Email: ziqing.zhai@rbm.qse.tohoku.ac.jp

On the other hand, it is well known that LAS is susceptible to thermal ageing emebrittlement during prolonged exposure in the 375 - 600ºC range. The cause of this embrittlement is attributed to GB segregation of nonmetallic impurities of groups IV – VI, essentially phosphorus (P) but also tin, antimony and arsenic [5]. Segregation of P to GBs in LAS is a relatively common occurrence in reactor pressure vessel steels and has been observed in base material, weld metal, and HAZ [6]. In addition, P segregation was found to promote IGSCC of ferritic steels in caustic [7] and nitrate [8] solutions. Although so far no segregation-induced failure has been reported in BWRs, possible synergism may exist between thermal ageing (especially P segregation) and SCC after extending reactor operation life up to 60 years or more. To date, little knowledge is available on this aspect and further investigation is necessary for the evaluation/extension of plant service time.
Therefore in this study, a systematic approach is carried out to clarify the potential synergism between thermal ageing, represented by P segregation and SCC in the HAZ of an A182-A533B DWJ, with a special focus on HAZ microstructure. SCC behavior in HAZ was investigated by creviced-bent beam (CBB) test, and the results were quantitatively correlated to the data on P segregation, which was obtained in a previous study, to evaluate the thermal ageing effects on SCC susceptibility

in the HAZ of LAS.

2. Experimental

2.1 Materials and Heat Treatments

The HAZ investigated in this study was fabricated by filling A182 into a machined groove in an A533B plate using shielded arc welding. The chemical compositions of the LAS base metal (BM) and A182 weld metals are given in

Table **1**. A typical post-weld heat treatment (PWHT) at 615 ºC for 25 h was applied to reduce residual stresses present after the welding and fast cooling process. An additional step cooling treatment was conducted on part of the weld joint to enhance P segregation [9]. The sequence for this process was 593 ºC/1 h → 538 ºC/15 h →524 ºC/24 h → 496 ºC/48 h → 468 ºC/125 h.

2.2 Microstructural Characterization

Etching was applied to identify the microstructural morphologies in HAZ. Plate specimens containing the DWJ from both non step-cooled (NSC) and step-cooled (SC) materials were used for this purpose. After grinding by emery paper up to 1000 grit, the specimens were polished in four steps with a diamond paste of 9 μm, 6 μm, 3 μm and 1 μm granulation consecutively. Then the specimens were immersed in picric acid-based aqueous solution at room temperature for 3 min to reveal the microstructures of HAZ.

2.3 CBB Test

In order to evaluate the SCC behavior on a general basis, CBB test was selected for its potential of producing a large number of cracks and its constant small strain which can enable a more delicate investigation on crack retardation and reactivation.

As shown in Fig.1(a), two types of specimens of size L35 mm × W8 mm × T2 mm were prepared from both NSC and SC materials. The first type contains the DWJ with a very thin layer (< ~ 500 μm) of A182 at the top from which cracks are expected to initiate and grow in the direction perpendicular to FB, while the second type contains only BM of LAS. It should be noted that in the DWJ specimens, the distance from specimen surface to the FB is not constant but fluctuates continuously with weld passes. Cold work is introduced at the top surface of A182 by roughly grinding the specimens with emery paper up to 120 grit, in order to accelerate crack initiation in A182. The specimens were then cleaned with acetone in ultrasonic washer, and fastened in pair onto each stage of the test fixtures (Fig.1(b)). The upper and lower surface of the fixtures contacting the specimens are in concave and convex form respectively, producing a small uniform tensile strain at the top surface of specimens. A piece of graphite fiber wool was placed on the top surface of the specimens to accelerate the corrosion by forming crevice environment.

In total, two sets of specimens were prepared. Each group consisted of one DWJ and one BM specimen from both the NSC and SC materials. The CBB test was conducted in 288˚C water with 8 ppm dissolved oxygen at 10 MPa. The flow rate was kept around 0.5 autoclave exchange per hour. At the first stage of the test, the two groups of specimens were subjected to 1% surface strain and exposed in water doped with 1 ppm SO_4^{2-} (added as Na_2SO_4). After 1000 h of immersion, all specimens were taken out, washed and reloaded to new jigs to increase the surface strain to 2%. While one group of specimens (hereafter referred to as G1) remained in the same autoclave with 1 ppm SO_4^{2-} addition, the other group (hereafter referred to as G2) was moved to another

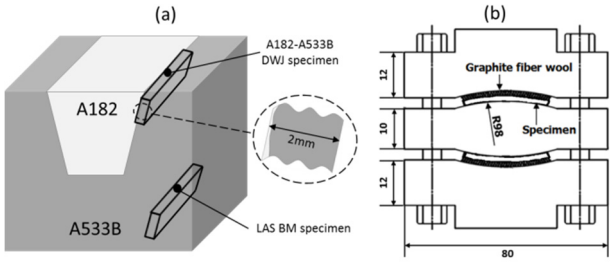

Fig.1 (a) The sampling location of specimens, and (b) the configuration of test fixtures for the CBB test.

Table 1. The chemical compositions of LAS base metal and A182 weld metals (wt.%).

	C	Si	Mn	P	S	Ni	Cr	Mo	Cu	V	Co	Ti	Nb + Ta	Fe
A533B	0.20	0.24	1.41	0.009	0.004	0.65	0.13	0.54	0.12	0.001	/	/	/	Bal.
Inconel 182	0.053	0.44	6.50	0.004	0.002	68.90	14.70	/	/	/	/	0.52	1.55	7.23

Yamada weld 182	0.033	0.65	5.70	0.011	0.006	69.95	13.85	/	0.01	/	0.01	0.60	1.70	6.98

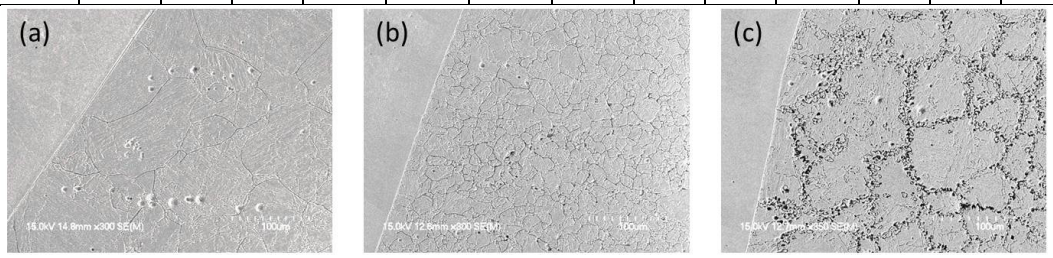

Fig.2 HAZ microstructures in the immediate vicinity of the FB: (a) CGHAZ, (b) FGHAZ, and (c) ICCGHAZ

(added as NaCl). After another 1000 h of immersion, the specimens were taken out, washed and sliced into three pieces along the longitudinal direction. Two pieces from each specimen were embedded in epoxy from which their cross-sections were observed.

In order to collect sufficient data on crack reactivation/ propagation in HAZ, all the mounted specimens were attenuated carefully by ~100 μm for five times consecutively. The surfaces of the specimens were observed under optical microscope after each time of attenuation, giving a total observed FB length of 350 mm for each combination of water chemistry and material conditions. Care was taken to ensure that a similar surface area was observed for each type of the HAZ microstructures in the immediate vicinity of FB identified with etching.

3. Results and Discussions

3.1 HAZ Microstructures

The entire HAZ with an average extension of 2–2.5 mm from FB was revealed after etching. In particular, complex phase transformations took place in the immediate vicinity of the FB (approximately 150–200 μm in width) due to the multiple thermal cycles induced by welding. Typically, three types of microstructures, namely coarse-grained HAZ (CGHAZ), fine-grained HAZ (FGHAZ) and intercritically reheated CGHAZ (ICCGHAZ), can be identified in this region, as presented in Fig.2. The CGHAZ consists of enlarged prior-austenite grains (~50–100 μm in size) from the second weld pass that grow rapidly due to being reheated to a temperature close to the melting point. The FGHAZ contains fine grains (~10–30 μm in size) resulting from slower austenitic grain growth at lower temperatures above A_{c1}. The ICCGHAZ is the region which has been reheated into the A_{c3} and A_{c1} transformation zone, featuring precipitation of very fine ferrite/austenites (≤ 5 μm) along prior-austenite GBs. These three types of microstructures generally occur in a fixed order along each weld pass, each extending ~300–500 μm along the FB to a distance of ~150–200 μm away from the FB. The result showed that the microstructural morphologies were not influenced by the step cooling process.

3.2 SCC Behavior in A182

Fig.3 presents the typical surface view and cross-section view of BM and HAZ specimens. Non-uniform corrosion prevails on the surface of BM specimen without specific penetration into LAS, suggesting little susceptibility of SCC in the BM of LAS at the tested conditions. On the contrary, a large number of cracks were initiated on the thin layer of A182 in DWJ specimens. Fig.4 summarizes the number of cracks initiated in A182 classified according to their lengths. Cracks of length shorter than 10 μm were not counted. The two groups of specimens exposed to different water indicating SCC was promoted by step cooling, in which GB microchemistry may have played an important role. Unfortunately, no composition analysis was performed on A182 in this study. From the limited data on the correlation between SCC susceptibility and GB microchemistry of Ni-base alloys, the major changes along GBs involve P segregation and Cr depletion. It is suggested that the segregated P is not detrimental but beneficial to the IGSCC resistance in as-welded A182 [10] and Alloy 600 [11] in high temperature waters. It is also reported that GB precipitates may [10] or may not [11] affect IGSCC in the above-mentioned Ni-base alloys. Further investigation is needed to attain a better understanding on why SCC in A182 was promoted by step cooling.

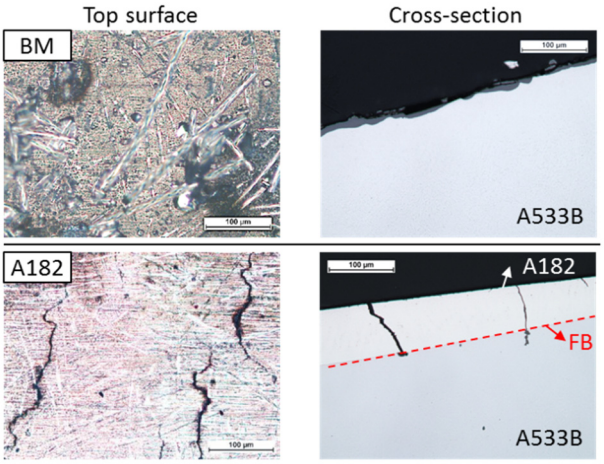

Fig.3 Typical morphologies of specimens after the CBB test (upper: BM, lower: DWJ)

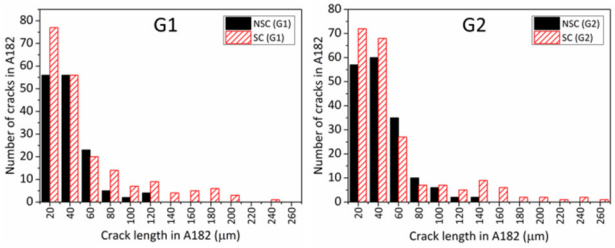

Fig.4 Distribution of the number and length of cracks initiated in A182 in DWJ specimens

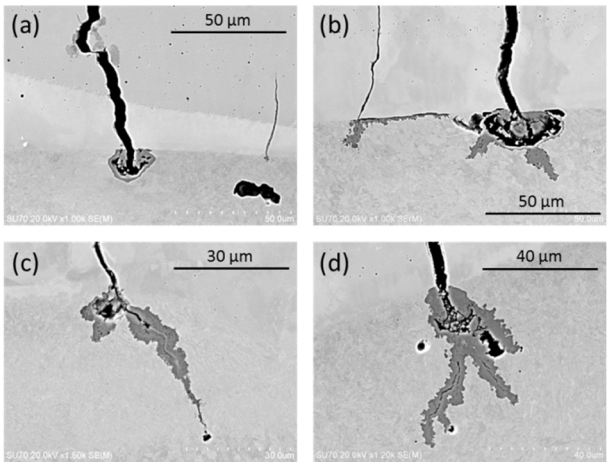

Fig.5 Classification of typical morphologies of the cracks reached FB

3.3 SCC behavior in HAZ

Once the cracks initiated in A182 reached the FB, oxidation was greatly promoted due to the sharp change in composition. As presented in Fig.5, several morphologies can be identified after the cracks reached FB: (a) cracks retarded by forming spherical oxides; (b) cracks propagating along the FB; (c) cracks propagating directly into the LAS; and (d) cracks reactivated from spherical oxides. Table 2 summarizes the fraction and total number of each type of cracks according to water chemistries and thermal histories. While most of the cracks were retarded by forming spherical oxides in the water doped with 1 ppm SO_4^{2-} only, the fraction of crack-like oxides and reactivated oxides were greatly promoted with the addition of 10 ppb Cl^-. This result is consistent with the reported role of Cl^- in accelerating crack initiation and growth using compact tension specimens [12].

The cross-sections of specimens were also etched to examine the microstructural characteristics of crack propagation path. As presented in Fig.6, the cracks in HAZ show mixed IG-TG morphologies. Two types of path are found to prefer crack reactivation and propagation in HAZ. The first type propagates along GBs (hereafter referred to as Type 1). This is consistent with the localized oxidation at GBs reported in other studies [2-4]. The second type aligns with certain packet (hereafter referred to as Type 2). It should be noted that the oxidized region at the tip and the both sides of the Type 2 cracks are too broad to allow accurate identification of the crack path. However, etching reveals that such cracks seem to propagate between laths inside the packet of which the alignment direction is approximately normal to the direction of the tensile strain exerted on the specimens. This is perhaps caused by the cementites aggregating at inter-lath region, since cementites normally act cathodically to adjacent ferrite, which can localize the electrochemical reactions that are necessary for crack reactivation/propagation [13]. In addition, it is well known that the coarse cementites are detrimental to the tensile properties and impact toughness of LAS [14, 15].

Table 3 summarizes the length of IG cracks and the fraction of IG failures, which equals the ratio of the total length of IG cracks to all cracks, with respect to HAZ microstructures. In the two groups of specimens, the IG fraction follows the trend: ICCGHAZ > CGHAZ > FGHAZ.

Table 2. Total number and fraction of each type of the crack morphologies observed in HAZ.

	NSC (G1)		SC (G1)		NSC (G2)		SC (G2)	
Spherical oxides	251	90%	90	70%	18	28%	81	50%
Cracks along FB	6	2%	11	9%	12	19%	14	9%
Crack-like oxides	17	6%	6	5%	18	28%	31	19%
Reactivated oxides	6	2%	22	17%	16	25%	37	23%

Table 3. Fraction of IG failure and the average length of IG cracks in different HAZ microstructures.

	ICCGHAZ		FGHAZ		CGHAZ	
NSC (G1)	80%	25.61 μm	41%	20.32 μm		
SC (G1)	88%	24.14 μm	60%	41.70 μm	70%	39.27 μm
NSC (G2)	71%	41.18 μm	46%	29.81 μm		
SC (G2)	69%	33.66 μm	50%	20.03 μm	60%	30.98 μm

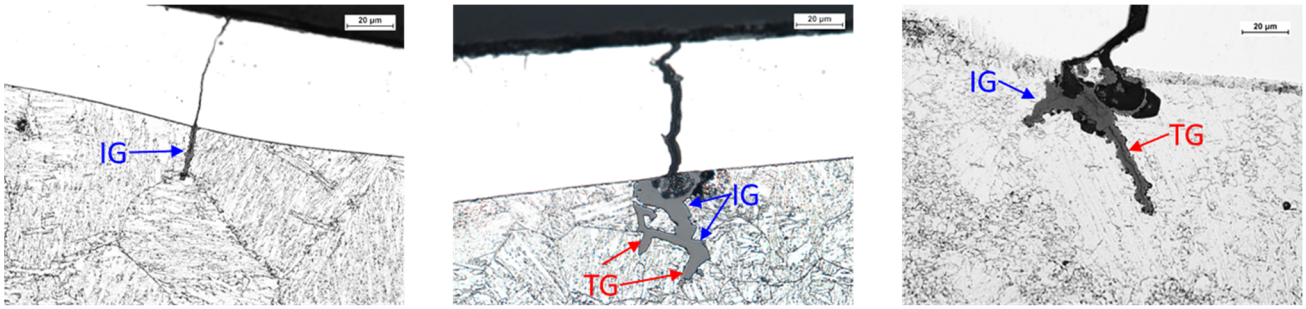

Fig.6 Crack paths revealed by etching

3.4 Correlation between Segregation and SCC Susceptibility in HAZ

The segregation behavior was investigated using atom probe tomography (APT) on ICCGHAZ, FGHAZ, CGHAZ and BM separately. The experimental procedure and detailed analysis are presented elsewhere [16, 17]. In brief, APT test results showed that P is the primary segregant at both G/PBs and P-M interfaces. Welding/PWHT and subsequent cooling, as well as step cooling have all contributed to the final level of P segregation at these two sites. Before step cooling, the segregation level of P at grain/packet boundaries (G/PBs) appears to depend on microstructure, being higher in CGHAZ and ICCGHAZ than in FGHAZ. The segregation level of P at P-M interfaces seems to depend on the type of precipitates: Al-Si rich precipitate > Mo-rich M_2C carbide > cementite. After step cooling, the segregation level of P was enhanced at G/PBs in all HAZ microstructures and
at cementite-matrix interfaces. Segregation of C, Mn and Mo were also observed at G/PBs in both the NSC and SC materials. After step cooling, the segregation level of Mn was increased while those of C and Mo were reduced.

As shown in Fig.7, for the two sets of CBB test under different water chemistries, the length and the number of crack-like oxides and reactivated oxides are more elevated in SC specimens. Although chloride has been demonstrated to promote SCC in this study, it should be noted that chloride usually induces TGSCC by activating dissolution at slip planes [18]. The existence of IG cracks cannot be explained by the doped impurities in water. In addition, SCC crack growth did not occur at stress intensity factor as high as 60 MPa $m^{1/2}$ in pre-cracked compact tension specimens with steel sulphur content equivalent or higher than the LAS investigated in this study [12]. On the other hand, galvanic corrosion has been proposed to explain the enhanced oxidation in HAZ [3, 4]. However, this effect is confined within very limited region beneath the FB, and is more likely to result in pitting and oxidation along FB. Therefore, microstructure and microchemistry seem to play the primary role in the crack reactivation/ propagation in HAZ.

Since HAZ microstructures are similar in NSC and SC materials, and step cooling does not alter the carbide

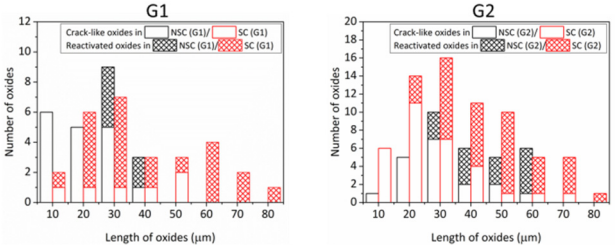

Fig.7 Distribution of the number and length of crack-like oxides and reactivated oxides in the HAZ

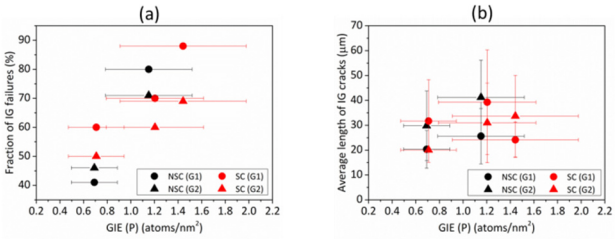

Fig.8 Correlation between the GIE of P at G/PBs and (a) the fraction of IG failure and (b) the average length of IG cracks observed in the HAZ of CBB specimens

distribution produced by PWHT [19], changes in microchemistries at preferential paths for crack reactivation/propagation, i.e., G/PBs and P-M interfaces are most likely the cause for the increased SCC incidences observed after step cooling. For the case of SCC propagating along G/PBs, the changes in the segregation level of P, C and Mo before and after step cooling are of interest. To the author's knowledge, the effects of these elements on SCC have only been investigated in caustic solution for iron based alloys. The results clearly demonstrated that segregated P is the primary cause for IGSCC, while the additions of Mo and C have a much lesser but still detrimental effect on the SCC resistance of these alloys [7]. In particular, it is believed that the presence of P and Mo at GBs can alter the oxide film across the GBs and allow IG crack propagation to proceed. If this is the case in high temperature water, the decreased segregation level of C and Mo observed at G/PBs after step cooling would be beneficial to the SCC resistance of LAS. Hence P seems to be the most deleterious segregant for SCC in HAZ in the SC material. This is in agreement with Fig.8, where the Gibbsian interfacial excess (GIE) [20] of P shows linear relationship with both the fraction of IG failure and the average IG crack length in HAZ, indicating that P plays an important role in increasing the IGSCC susceptibility in the tested environments. As LAS is usually passive at the elevated potentials susceptible to SCC, the reactivation and propagation of SCC require continuous active paths and sufficient stress to prevent blockage of the crack by corrosion products. P has been demonstrated to interact with SCC by electrochemical tests on LAS in hot caustic/nitrate solutions. Depending on environmental conditions and steel composition, segregated P at GBs can either dissolve into phosphorus ions, accelerating the anodic dissolution that lowers corrosion potential and raises passivation potential [8]; or into phosphate ions, which would redeposit onto crack sides, enhance passivity, thus keep the crack tip sharp and prevent crack tip blunting [19]. On the other hand, from a mechanical point of view, segregated P can facilitate IG fracture through a reduction in GB cohesion.

In addition, preferential P segregation at P-M interfaces has been reported to reduce the interfacial strength, accelerating embrittlement [21] and TG crack growth [22]. As P was found to segregate to P-M interfaces in this study, it seems reasonable to deduce that the TGSCC observed in alignment with certain packet mainly follows the interface between cementites and ferrite laths. It is also possible that the enhanced P segregation at interfaces between GB precipitates and matrix promoted TGSCC in SC specimens.

Since the enhanced P segregation at G/PBs induced by step cooling can also be attained or even surpassed by equilibrium segregation during thermal ageing, the above discussion suggests that thermal ageing may affect SCC susceptibility in HAZ by altering the microchemistry at G/PBs and P-M interfaces, especially through P segregation. SCC tests on isothermally aged materials would provide additional valuable information on the effects of P segregation on SCC in HAZ in progress with time.

4. Conclusions

(1) Etching revealed that the HAZ microstructure in the immediate vicinity of FB can be classified into CGHAZ, FGHAZ and ICCGHAZ. The matrixes in these

regions are generally of upper bainitic structure.

(2) CBB test showed that there are four possibilities after a crack initiated in A182 reach the FB: retarded by forming spherical oxide, propagating along the FB, propagating directly into HAZ, or reactivated from spherical oxide. It is also suggested that Cl^- induced more crack reactivation/propagation in HAZ than SO_4^{2-}.

(3) Both TGSCC and IGSCC were observed in HAZ. Crack reactivation/propagation seems to prefer either GBs or to align with certain packets. However, the cracks were only found within limited region in HAZ and did not show obvious propensity of growing into the base metal.

(4) SCC reactivation/propagation in HAZ was promoted by step cooling, which seems due primarily to the P segregation at G/PBs (contributing to IGSCC along GBs) and at P-M interfaces (contributing to TGSCC in alignment with certain packets). It is indicated that long-term thermal ageing would increase the SCC susceptibility in HAZ.

References

[1] "Assessment and Management of Ageing of Major Nuclear Power Plant Components Important to Safety: BWR Pressure Vessels", IAEA, Vienna, Austria: 2005. IAEA-TECDOC-1470; p127.

[2] H. Abe, M. Ishizawa and Y. Watanabe, "Stress corrosion cracking behavior near the fusion boundary of dissimilar weld joint with Alloy 182-A533B low alloy steel", 15th International Conference on Environmental Degradation of Materials in Nuclear Power Systems-Water Reactors, 2012, pp.791-802.

[3] J. Hou, Q. Peng, Y. Takeda, J. Kuniya and T. Shoji, "Microstructure and stress corrosion cracking of the fusion boundary region in an alloy 182-A533B low alloy steel dissimilar weld joint", Corrosion Science, Vol.52, 2010, pp.3949-3954.

[4] Q. Peng, H. Xue, J. Hou, K. Sakaguchi, Y. Takeda, J. Kuniya and T. Shoji, "Role of water chemistry and microstructure in stress corrosion cracking in the fusion boundary region of an Alloy 182-A533B low alloy steel dissimilar weld joint in high temperature water", Corrosion Science, Vol.53, 2011, pp.4309-4317.

[5] M. Guttmann, "Interfacial Segregation and Temper Embrittlement", in "Encyclopedia of Materials: Science and Technology (Second Edition)", Elsevier, 2001; pp.1 - 8.

[6] C.A. English, S.R. Ortner, G. Gage, W.L. Server and S.T. Rosinski, "Review of phosphorus segregation and intergranular embrittlement in reactor pressure vessel steels", Effects of Radiation on Materials: 20th International Symposium, Manchester, U.K., 2000, pp.151-173.

[7] N. Bandyopadhyay and C.L. Briant, "Caustic stress corrosion cracking of low alloy iron base materials", Corrosion, Vol.41, 1985, pp.274-280.

[8] J. Küpper, H. Erhart and H.-J. Grabke, "Intergranular corrosion of iron-phosphorus alloys in nitrate solutions", Corrosion Science, Vol.21, 1981, pp.227-238.

[9] C. Naudin, J.M. Frund and A. Pineau, "Intergranular fracture stress and phosphorus grain boundary segregation of a Mn-Ni-Mo steel", Scripta Materialia, Vol.40, 1999, pp.1013-1019.

[10] Q. Peng, J. Hou, Y. Takeda and T. Shoji, "Effect of chemical composition on grain boundary microchemistry and stress corrosion cracking in Alloy 182", Corrosion Science, Vol.67, 2013, pp.91-99.

[11] G.S. Was, J.K. Sung and T.M. Angeliu, "Effects of grain boundary chemistry on the intergranular cracking behavior of Ni-16Cr-9Fe in high-temperature water", Metallurgical Transactions A, Vol.23, 1992, pp.3343-3359.

[12] H.P. Seifert and S. Ritter, "Stress corrosion cracking of low-alloy reactor pressure vessel steels under boiling water reactor conditions", Journal of Nuclear Materials, Vol.372, 2008, pp.114-131.

[13] J.A.S. Green and R.N. Parkins, "Electrochemical properties of ferrite and cementite in relation to stress corrosion of mild steels in nitrate solutions", Corrosion, Vol.24, 1968, pp.66-69.

[14] S. Kim, S. Lee, Y.-R. Im, H.-C. Lee, Y. Oh and J. Hong, "Effects of alloying elements on mechanical and fracture properties of base metals and simulated heat-affected zones of SA 508 steels", Metallurgical

and Materials Transactions A, Vol.32, 2001, pp.903-911.

[15] Y.-R. Im, B.-J. Lee, Y.J. Oh, J.H. Hong and H.-C. Lee, "Effect of microstructure on the cleavage fracture strength of low carbon Mn–Ni–Mo bainitic steels", Journal of Nuclear Materials, Vol.324, 2004, pp.33-40.

[16] Z. Zhai, Y. Miyahara, H. Abe and Y. Watanabe, "Segregation behavior of phosphorus in the heat-affected zone of an A533B/A182 dissimilar weld joint before and after simulated thermal aging", Journal of Nuclear Materials, Vol.452, 2014, pp.133-140.

[17] Z. Zhai, Y. Miyahara, H. Abe and Y. Watanabe, "Effects of thermal history and microstructure on segregation of phosphorus and alloying elements in the heat-affected zone of a low alloy steel", Metallurgical and Materials Transactions A, Vol.under review.

[18] C. Lea and E.D. Hondros, "Intergranular microchemistry and stress corrosion cracking", Proceedings of the Royal Society of London. A. Mathematical and Physical Sciences, Vol.377, 1981, pp.477-501.

[19] N. Bandyopadhyay and C.L. Briant, "Caustic stress corrosion cracking of NiCrMoV rotor steels-The effects of impurity segregation and variation in alloy composition", Metallurgical and Materials Transactions A, Vol.14, 1983, pp.2005-2019.

[20] M.K. Miller and G.D.W. Smith, "Atom probe analysis of interfacial segregation", Applied Surface Science, Vol.87–88, 1995, pp.243-250.

[21] "Materials Reliability Program: A Review of Thermal Aging Embrittlement in Pressurized Water Reactors (MRP-80)", EPRI, Palo Alto, CA: 2003. 1003523.

[22] C.A. Hippsley and C.E. Lane, "Hydrogen embrittlement, thermal aging, and role of carbides in fatigue of high strength steel", Materials Science and Technology, Vol.6, 1990, pp.735-742.